Chemico-Biological Interactions 396 (2024) 111042

Contents lists available at ScienceDirect

Chemico-Biological Interactions

journal homepage: www.elsevier.com/locate/chembioint

Research paper

Cytotoxicity of acridinium-based ionic liquids: Structure-activity relationship and mechanistic studies

Ritik Roy, Phoenix Chick, Edward York, Tristan Rawling *

School of Mathematical and Physical Sciences, Faculty of Science, University of Technology Sydney, Sydney, NSW, 2007, Australia

ARTICLE INFO

Keywords:
Ionic liquid
Cytotoxicity
Mitochondria
Structure activity relationship
Acridine

ABSTRACT

Ionic liquids (ILs) are a class of low melting point salts with physicochemical properties suitable for a range of industrial applications such as chemical processing and battery design. Major challenges to the wide-scale adoption of ILs in industry include their eco- and cytotoxic effects, however, this opens up the possibility of the use of ILs use as novel anticancer agents. Understanding the structural features that promote IL cytotoxicity is therefore important. Key structural features that can impact IL cytotoxicity include size and lipophilicity of the cationic head group. In this study, the cytotoxic effects of acridinium-based ILs containing relatively large tri- and tetracyclic cations were evaluated. It was found that 9-phenylacridinium-based ILs are potent cytotoxic agents that reduce the viability of human MDA-MB-231 breast cancer cells with IC_{50} concentrations in the nanomolar range. In mechanistic studies, it was found that unlike the pyridinium-based analogue, $[C_{16}Py][I]$, acridinium-based ILs did not inhibit oxidative phosphorylation or induce reactive oxygen species formation, and may instead target other mitochondrial processes or components such as mitochondrial DNA.

1. Introduction

Ionic liquids (ILs) are a class of low melting point ionic compounds comprised of inorganic anions and bulky organic cations, which are frequently substituted with one or more *N*-alkyl side chains. Due to their high thermal stability and low flammability, ILs have been explored as safe and environmentally friendly alternatives to conventional solvents for a wide range of applications in fields including energy storage and chemical processing [1]. The low volatility, incompressibility, chemical stability, and viscosity–temperature properties of ILs also make them attractive lubricants [2]. As interest in ILs has grown over the past few decades, it has become apparent that ILs are not as benign as previously thought. Indeed, numerous studies have shown that ILs are cytotoxic towards microorganisms [3], marine organisms [4,5]. murine cells [6–8], and human cancer cells [9–12]. From a medicinal chemistry perspective, ILs are an attractive option for novel cancer therapeutics as they have a balance of polar and lipophilic properties required for an acceptable pharmacokinetic profile, and they appear to kill cancer cells by novel mechanisms. A detailed understanding of the mechanism/s and structural features that promote IL cytotoxicity will be an important part of their future development for industrial applications or as therapeutic agents.

Structure activity relationship (SAR) studies of ILs have revealed some features of ILs that modulate their cytotoxicity. Firstly, the *N*-alkyl side chain attached to the cationic head group is the greatest determinant of activity, where increased chain length leads to an increase in cytotoxicity [5–12]. Secondly, the inclusion of polar substituents in the *N*-alkyl chain decreases activity, suggesting that greater head group polarity lowers potency [12]. [[,13] Lastly, the nature of the anion has minimal impact on activity, although the bis(trifluoromethylsulfonyl) imide (NTf_2) anion appears to promote cytotoxicity in some cases [9,10, 14]. The impact of the structure of the cationic head group has been less well reported. Several studies have shown that ILs with aliphatic head groups are less cytotoxic than those bearing aromatic cations [10,13, 15], however further findings have been limited by the low structural diversity of ILs employed in toxicity studies. In a recent study that sought to expand the SAR, we synthesised a series of amphiphilic ionic liquids (AmILs) – ILs with lipophilic *N*-alkyl chains – containing structurally diverse head groups and assessed their capacity to reduce the viability of human MDA-MB-231 breast cancer cells [16]. It was found that head group size and lipophilicity were key structural features that affected activity. For example, substitution or fusion of additional phenyl rings onto the pyridinium-based head group of $[C_{16}Py][I]$ (see Fig. 1) increased its cytotoxicity by approximately 4.8-fold [16]. This

* Corresponding author. School of Mathematical and Physical Sciences, Faculty of Science, University of Technology Sydney, Ultimo, NSW, 2007, Australia.
E-mail address: Tristan.Rawling@uts.edu.au (T. Rawling).

https://doi.org/10.1016/j.cbi.2024.111042
Received 18 January 2024; Received in revised form 25 April 2024; Accepted 5 May 2024
Available online 10 May 2024

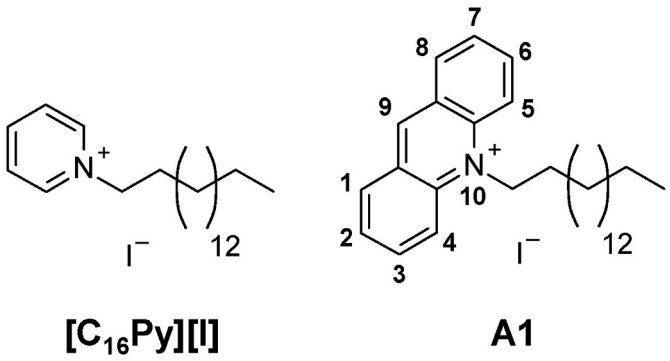

Fig. 1. Chemical structures of 1-hexadecylpyridinium iodide [C_{16}Py][I] and 10-hexadecylacridinium iodide (**A1**). [C_{16}Py][I] has previously been shown to induce mitochondrial dysfunction in MDA-MB-231 cells [16].

has important implications for the use of ILs as pharmaceutical agents and industrial materials, as AmILs with relatively large and highly symmetric cations are being researched as lubricants for their suitable rheological properties including low volatility and high viscosity [2,17].

Our previous SAR study was limited largely to ILs bearing mono- and bicyclic cationic head groups. In this study we extended the head group size to tri- and tetracyclic acridinium-based ILs and assessed their cytotoxicity against MDA-MB-231 cells. The impacts of head group substitution were also assessed as this area has received little attention in the literature. We also assessed the capacity of two acridinium-based AmILs to permeabilise lipid membranes and induce mitochondrial dysfunction, as these are associated with the mechanisms by which AmILs exert cytotoxicity [6,10,11,16,18,19]. From these studies it was found that tetracyclic 9-phenylacridinium based ILs are highly cytotoxic agents that appear to induce cell death by a different mechanism to that of ILs with smaller head groups, which may involve targeting of DNA.

2. Materials and methods

2.1. Reagents

Acridine, calf thymus DNA (CT-DNA), diphenylamine, *p*-tolylamine, propionic acid, Dulbecco's Modified Eagle Medium (DMEM), penicillin and streptomycin, phosphate-buffered saline (PBS), DMSO, and all biochemicals, benzoic acids, and anhydrous solvents were purchased from Sigma-Aldrich (Castle Hill, NSW, Australia) and used as is. All remaining reagents were purchased from Fluorochem (Hadfield, Derbyshire, United Kingdom) and used as is. Fetal bovine serum (FBS) and trypsin/EDTA were purchased from Invitrogen, Life Technologies (Mulgrave, Victoria, Australia). 2-Dioleoyl-*sn*-glycero-3-phosphocholine (DOPC) was purchased from Avanti Polar Lipids Inc. (Alabaster, Alabama, USA).

2.2. Synthesis

All synthetic procedures and characterisation data are provided in detail in the Supporting Information. Purity of all test compounds was confirmed to be >95 % by absolute quantitative ^{1}H NMR analysis, as previously described by Pauli et al. [20] This technique determines purity by calculating the proportionality between ^{1}H NMR signals against an internal reference calibrant (see Supporting Information).

2.3. Tethered bilayer lipid membrane (tBLM) experiments

Tethered lipid bilayers were anchored across a gold electrode with 'T10' architecture, consisting of 10 % benzyl-disulfide (tetra-ethylene glycol) n = 2C_{20}-phytanyl interspacing "tethers" with 90 % benzyl-disulfide-tetra-ethylene-glycol-OH "spacer" molecules [21]. Spacer and tether molecules were coordinated onto a 2.1 mm^2 gold tethering electrode. To the initial layer was added a second layer of mobile phase lipid molecules of 3 mM DOPC (Avanti Polar Lipids Inc., Alabama, USA). The layers were left to incubate at room temperature for exactly 2 min before a rapid exchange of 3 x 200 μL 100 mM NaCl Tris buffer to induce the formation of a complete tBLM.

Swept frequency (0.1–2000 Hz) electrical impedance spectroscopy was applied at 25 mV peak-to-peak using a Tethapod™ impedance spectrometer (SDx Tethered Membranes Pty Ltd, NSW, Australia). Impedance and phase profiles were fitted to an equivalent circuit consisting of a tethering gold electrode and reservoir region connected in series with a resistor to represent the impedance of the surrounding electrolyte solution, and a resistor/capacitor representing the lipid bilayer (as previously described) [22]. Data were fitted using an adapted Levenberg-Marquardt fitting method incorporated into the Tetha-Quick™ software (SDx Tethered Membranes Pty Ltd, NSW, Australia).

2.4. General cell culture

Human MDA-MB-231 breast cancer and BEAS-2B bronchial epithelial cells were obtained from American Type Culture Collection (Manassas, Virginia, USA). MDA-MB-231 cells were grown at 37 °C in a humidified atmosphere of 5 % CO_2 in DMEM supplemented with 10 % FBS and 1 % penicillin/streptomycin. Confluent cells (80–90 %) were harvested with trypsin/EDTA after washing with PBS. BEAS-2B cells were grown at 37 °C in a humidified atmosphere of 5 % CO_2 in DMEM supplemented with 10 % FBS. Confluent cells (80–90 %) were harvested with trypsin/EDTA after washing with PBS.

2.5. MTS cell viability assay

MDA-MB-231 or BEAS-2B cells were seeded in triplicate in clear bottom 96-well plates (5 × 10^3 cells per well) and incubated overnight. After 24 h the media was removed, and cells were treated with various concentrations of the test compounds in DMSO (final concentration 0.1 %) and incubated for 48 h. Cells were then incubated with CellTiter MTS 96® Aqueous MTS Reagent Powder (Promega) and phenazine ethosulfate (Sigma-Aldrich) under dark conditions for 3 h. The absorbance of each well at 490 nm was measured using a Tecan Infinite M1000 Pro plate reader to evalute cell viability according to the manufacturer's recommendation (CellTiter 96® Aqueous One Solution Cell Proliferation Assay, Promega, Wisconsin, USA). MTS IC50 values were defined as the drug concentration that prevented more than 50 % of cell growth (relative to the control) and determined using nonlinear regression analysis with Prism 8.4.3 (GraphPad Software, California, USA).

2.6. Seahorse XF analysis

Seahorse XF sensor cartridges were hydrated for 24 h prior to the experiments using Seahorse XF calibrant at 37 °C in a humidified non-CO_2 atmosphere. MDA-MB-231 cells were seeded in XF 24 cell culture microplates (2 × 10^4 cells per well) and incubated for 24 h in a humidified atmosphere of 5 % CO_2. The cells were washed twice with XF Base medium supplemented with 10 mM D-(+)-glucose, 2 mM L-glutamine and 1 mM sodium pyruvate at pH 7.4 prior to the final addition of 450 μL assay medium/well. The cells were incubated at 37 °C in a humidified non-CO_2 atmosphere for 1 h. The loaded XF sensor cartridge was placed into a Seahorse XFe24 Analyser and calibrated. Once calibrated, the calibration fluid was replaced with XF 24 cell culture microplates containing cells. Test compounds/DMSO (50 μL) were injected into designated wells and the first set of OCR measurements were recorded. After 3 cycles, oligomycin (1 μM), FCCP (2 μM), and rotenone/Antimycin A (0.5 μM) were successively injected into each well. OCR was measured using a cycling program where 3 measurements were recorded between each injection. Readings for the last of each 3 cycles were used for OCR data analysis. OCR parameters were

calculated as follows: post-treatment respiration = Basal OCR – Rotenone/Antimycin A OCR; Maximal respiration = FCCP OCR – Rotenone/Antimycin A OCR; ATP production = post-treatment respiration OCR – Oligomycin OCR.

2.7. JC-1 mitochondrial membrane potential assay

MDA-MB-231 cells were seeded in triplicate in 96-well black/clear bottom plates (1.5×10^4 cells per well) and incubated overnight. After 24 h, the media was removed and cells were treated with various concentrations of the test compounds in DMSO (final concentration 0.1 %) and incubated for 1 h. Cells were incubated with JC-1 for 20 min in media, washed with PBS (2 x 200 μL), and 200 μL of PBS was added to each well. The JC-1 red/green fluorescence ratio was measured using a Tecan Infinite M1000 Pro plate reader to determine red (595/535 nm) and green (535/485 nm) emmision/excitation wavelengths according to the manufacturer's recommendation (JC-1 Mitochondrial Membrane Potential Kit, Cayman Chemical, Michigan, USA).

2.8. Intracellular ATP assay

MDA-MB-231 cells were seeded in triplicate in 96-well black/clear bottom plates (1×10^4 cells per well) and incubated overnight. After 24 h the media was removed, and cells were treated with the test compounds in DMSO (final concentration 0.1 %) and incubated for the duration of the experiment. Cells were incubated with CellTiter-Glo® in media, mixed for 2 min in an orbital shaker, and left at room temperature under dark conditions for 10 min, after which luminescence was read using a Tecan Infinite M1000 Pro plate reader to quantify intracellular ATP levels according to the manufacturer's recommendation (CellTiter-Glo® 2.0 Luminescent Cell Viability Assay, Promega, Wisconsin, USA).

2.9. LDH release assay

MDA-MB-231 cells were seeded in triplicate in 96-well black/clear bottom plates (1×10^4 cells per well) and incubated overnight. After 24 h the media was removed, and cells were treated with the test compounds in DMSO (final concentration 0.1 %) and incubated for 6 h. Aliquots of treatment medium (3 μL) were taken from each well and combined with LDH storage buffer previously prepared according to the manufacturer's instructions (LDH-Glo™ Cytotoxicity Assay, Promega, Wisconsin, USA). The combined solutions were incubated with prepared LDH detection reagent at room temperature under dark conditions for 60 min and luminescence was read using a Tecan M1000 Pro plate reader to quantify levels of extracellular LDH according to the manufacturer's recommendation (LDH-Glo™ Cytotoxicity Assay, Promega, Wisconsin, USA). Values were standardised to cells lysed in cell media containing Triton X-100 (0.2 % v/v) and are expressed as a percentage of maximal LDH release.

2.10. DCFDA assay

MDA-MB-231 cells were seeded in triplicate in 96 well black/clear bottom plates (2×10^4 cells per well) and incubated overnight. After 24 h the media was removed, and cells were treated with 100 μL of 20 μM DCFDA solution (prepared in phenol red-free and serum-free DMEM) and incubated for 25 min. Each well was washed with PBS (2 x 200 μL) and 100 μL of phenol red-free DMEM (1 % FBS) was added. Cells were treated with various concentrations of the test compounds in DMSO (final concentration 0.1 %) and incubated for 10 min. Fluorescence intensity was measured using a Tecan M1000 Pro plate reader to determine emission/excitation wavelengths at 529/495 nm. Fluorescence was continuously monitored and final readings during linear changes were reported with respect to time-matched DMSO-treated control cells.

2.11. Statistical analysis

All data are expressed as means ± SEM of 3 independent experiments (N = 3) unless otherwise specified. Normalised dose-response curves were constructed using GraphPad Prism 8.4.3 to calculate absolute and relative IC_{50} concentrations (see Supporting Information). ATP and LDH release data are expressed as means ± SEM of time-matched DMSO-treated and Triton X-100-treated controls, respectively, and were analysed by two-way ANOVA with Dunnett's multiple comparison test. DCFDA data are expressed as means ± SEM and were analysed by two-way ANOVA with Dunnett's multiple comparison test. Seahorse and tBLM data were normalised to baseline DMSO-treated controls prior to the addition of test compounds.

3. Results and discussion

3.1. Compound library design and synthesis

A library of acridinium-based AmILs was designed to investigate how structural modification of the cationic head group and *N*-alkyl chain affect cytotoxicity of AmILs towards MDA-MB-231 cells. Firstly, the impact of substitution at the 9-position of the acridinium head group was explored (**A1-3**, see Table 1), followed by a series of 9-phenyl-substituted derivatives to assess the impact of substitution at this ring (**A4-18**, see Table 1). **A4-18** were prepared as iodide salts with hexadecyl (C_{16}) chains so that the head group effects could be studied in isolation. To understand how the *N*-alkyl side chain affects activity, chain-shorted (C_{10}–C_{14}, **A19**–**21**) and chain-elongated (C_{18} and C_{20}, **A22** and **A23**) analogues of **A3** (C_{16}) were prepared (see Table 1).

The synthetic procedures used to prepare AmILs **A1-A23** are shown in Scheme 1. Substituted acridines **3a-l** were prepared using Bernthsen reactions, where diphenylamine **2a** or *p*-tolylamine **2b** was reacted with carboxylic acids **1a-j** in the presence of zinc chloride. Under these

Table 1
Chemical structures, melting points, and absolute MTS IC_{50} concentrations of **A1-23** measured in human MDA-MB-231 breast cancer cells (48 h treatment).

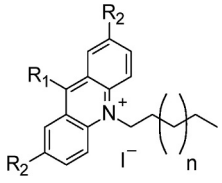

Cmpd	R_1	R_2	n	MTS IC_{50} [μM]	Melting point (°C)
A1	H	H	12	57.1 ± 3.7	110–113
A2	CH_2CH_3	H	12	56.0 ± 3.1	111–113
A3	Ph	H	12	0.76 ± 0.02	95–97
A4	*p*-CH_3Ph	H	12	0.80 ± 0.03	72–74
A5	*p*-CH_2CH_3Ph	H	12	1.1 ± 0.18	79–82
A6	*p*-$C(CH_3)_3$Ph	H	12	3.0 ± 0.03	78–80
A7	*p*-ClPh	H	12	1.6 ± 0.09	116–119
A8	*p*-CF_3Ph	H	12	4.9 ± 0.48	121–123
A9	*p*-OCF_3Ph	H	12	3.4 ± 0.46	101–104
A10	*p*-OCH_3Ph	H	12	0.71 ± 0.02	107–109
A11	*p*-$COCH_3$Ph	H	12	1.2 ± 0.06	97–100
A12	*p*-$COOCH_3$Ph	H	12	3.5 ± 0.16	106–108
A13	*m*-CH_3Ph	H	12	0.81 ± 0.02	70–73
A14	*o*-CH_3Ph	H	12	5.1 ± 0.95	62–66
A15	3,4-$(CH_3)_2$Ph	H	12	0.73 ± 0.06	96–100
A16	3,5-$(CH_3)_2$Ph	H	12	0.94 ± 0.14	124–128
A17	Ph	CH_3	12	1.5 ± 0.03	120–123
A18	*p*-CH_3Ph	CH_3	12	0.70 ± 0.02	117–120
A19	Ph	H	6	0.61 ± 0.04	65–68
A20	Ph	H	8	0.39 ± 0.03	72–75
A21	Ph	H	10	0.42 ± 0.05	87–90
A22	Ph	H	14	1.1 ± 0.02	103–105
A23	Ph	H	16	6.6 ± 0.03	108–111

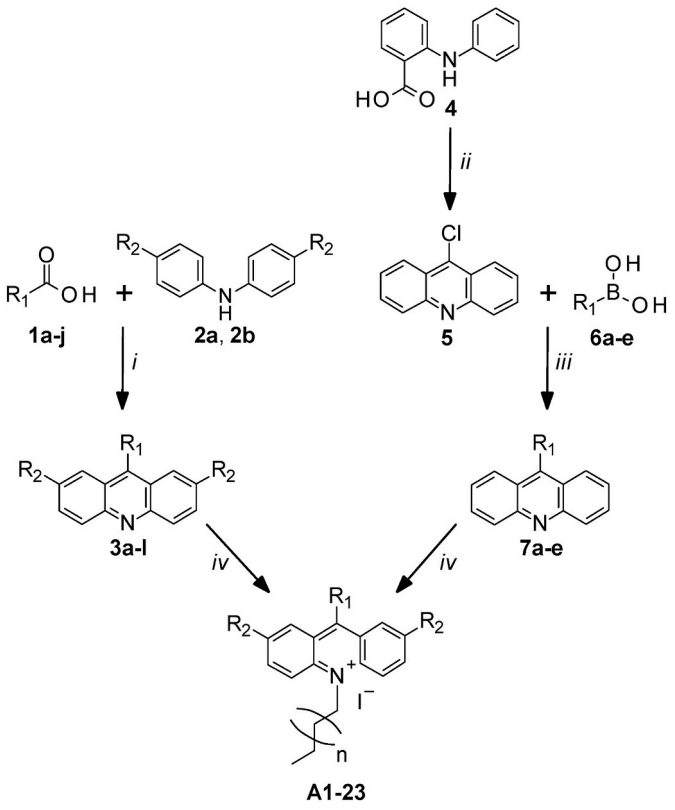

Scheme 1. Synthesis of acridinium-based AmILs **A1-23**. Reagents and conditions: (*i*) $ZnCl_2$, 220 °C, 20 h, 14–56 %; (*ii*) $POCl_3$, 100 °C, 4 h, 71 %; (*iii*) toluene, PCy_3, $PdOAc_2$, K_3PO_4, reflux, 17–24 h, 26–78 %; (*iv*) $CH_3(CH_2)_nI$, benzonitrile, 100 °C, 72–96 h, 4–54 %.

conditions, acid chlorides are generated *in situ* and undergo electrophilic addition with **2a** or **2b**, resulting with the formation of 9-substituted acridines. Bernthsen reactions using benzoic acids substituted with polar and electron-withdrawing substituents were not successful, thus 9-phenylacridines **7a-e** were synthesised using Suzuki-Miyaura cross-coupling reactions that make use of mild reaction conditions and display high functional group tolerance [23]. The aryl halide substrate for Suzuki-Miyaura reactions was 9-chloroacridine (**5**), which was prepared by the acid-catalysed cyclisation of *N*-phenylanthranilic acid (**4**). **5** was then coupled to phenylboronic acids **6a-e** using palladium (II) acetate as a catalyst to afford acridines **7a-e**.

The final step in the synthesis of **A1-23** was Menshutkin quaternisation reactions between acridines **3a-l**, **7a-e**, and the appropriate iodoalkanes, which were purchased commercially or prepared by reacting the corresponding bromoalkanes with sodium iodide. The quaternisation reactions were carried out in pressure tubes at 100 °C with benzonitrile as the solvent, and the desired products were precipitated from the reaction mixture by the addition of diethyl ether.

Melting points are an important physicochemical property of ILs and the melting point temperatures for all newly synthesised compounds are shown in Table 1. The melting point of acridinium-based IL **A1** was 110–113 °C, an inclusion of 9-phenyl group (**A3**) reduced the melting point by 15 °C. Mono-substitution of the 9-phenyl ring with alkyl groups (eg **A4**-**A6**, **A13**-**A14**) led to further reductions in melting points, while substitution with halogen or oxygen-containing function groups (**A7**-**A12**) produce compounds with melting points higher than **A3**. Comparison of **A4**, **A7** and **A8**, which possess substituents of similar size and lipophilicity, indicates that electron withdrawing substituents can increase melting point. As expected, the melting points of **A19**-**A23** clearly show and positive correlation with the length of the *N*-alkyl side chain, which can be attributed to increased Van der Waals interactions [24,25].

3.2. Effects of *A1-23* on MDA-MB-231 cell viability

The development of the acridinium-based AmILs series commenced with **A1**, which bears an unsubstituted acridinium head group. The corresponding pyridinium-based IL $[C_{16}Py][I]$ reduced MDA-MB-231 cell viability with an IC_{50} concentration of 7.7 ± 0.3 μM in MTS assays [16], and we anticipated that **A1** would have greater activity due to the increased size and lipophilicity of the acridinium head group. Surprisingly, **A1** was found to reduce MDA-MB-231 cell viability with an IC_{50} of 57.1 ± 3.7 μM under identical conditions (see Fig. S1 in Supporting Information for dose-response curve). To further increase head group size and lipophilicity, we explored substitution at the 9-position. The 9-ethyl substituted analogue **A2** was equipotent to **A1** (see Table 1), however inclusion of a 9-phenyl ring gave **A3**, which reduced MDA-MB-231 cell viability with an IC_{50} concentration of 0.76 ± 0.02 μM. The cytotoxicity of **A1** and **A3** was also assessed against a non-cancer cell line. **A1** and **A3** were found to reduce the viability of human BEAS-2B bronchial epithelial cells with IC_{50} concentrations of 8.9 ± 0.4 and 0.52 ± 0.04 μM, respectively, which suggests these ILs are less cytotoxic towards cancer cells.

Given its striking cytotoxicity, the structure of **A3** was modified at several positions to determine if further increases in activity could be achieved. AmILs **A4-14** are analogues of **A3** bearing different aromatic substituents in the 9-phenyl ring. **A4-14** reduced MDA-MB-231 cell viability with IC_{50} concentrations from 0.71 to 5.1 μM, which suggests that substitution of this ring produces only modest changes in potency. Analogues **A7**, **A8**, **A9**, **A11** and **A12** were ~1.5- to 6-fold less potent than **A3** and indicate that electron-withdrawing groups reduce activity. Substitution with one or two electron donating methyl groups in the *meta*- or *para*-positions of the 9-phenyl ring had negligible effects on potency, given that **A4** (*p*-CH_3), **A13**, (*m*-CH_3), **A15** (3,4-$(CH_3)_2$), and **A16** (3,5-$(CH_3)_2$) were equipotent to **A3**. Interestingly, the *ortho*-methyl-substituted analogue **A14** was 6-fold less potent than **A3** and all other methyl-substituted analogues, which indicates that only substitution at this position lowers cytotoxicity. This is significant as *ortho*-methyl groups in bicyclic systems can be used as conformational blockers to lock the two ring systems out-of-plane with each other. The reduced activity of **A14** therefore suggests that the cytotoxicity of 9-phenylacridinium-based ILs is greatest when the two ring systems are in-plane with each other.

The impact of methyl group substitution at positions 2 and 7 of the acridinium head group was also explored using compounds **A17** and **A18**. These AmILs reduced MDA-MB-231 cell viability with similar IC_{50} concentrations to their unsubstituted counterparts **A3** and **A4**, respectively. These findings are consistent with the observed effects of substitution in the 9-phenyl ring and suggest that the inclusion of methyl groups in the head group has negligible effects on activity, except when in the *ortho*-position of the 9-phenyl ring.

Lastly, modification of the C_{16} *N*-alkyl chain of **A3** was explored. Previous studies have consistently shown that AmIL cytotoxicity increases with *N*-alkyl chain length [5], [-12] which most likely occurs because the chain promotes accumulation of AmILs into cellular membranes. For example, increasing the butyl chain of $[C_4Py][Br]$ by 6 carbons to give $[C_{10}Py][Br]$ led to an ~ 150-fold increase in cytotoxicity towards HeLa cells, as well as a corresponding increase in the capacity of $[C_{10}Py][I]$ to permeabilise DOPC lipid bilayers [10]. Interestingly, within the acridinium-based series it was found that shortening the chain to C_{14} (**A21**), C_{12} (**A20**) or C_{10} (**A19**) had little impact on potency relative to **A3**, and increasing the chain length to C_{18} (**A22**) and C_{20} (**A23**) slightly lowered activity. These findings are unexpected and suggest that the acridinium-based ILs kill cells by a different mechanism of action that may not involve targeting of membranes.

3.3. Mechanistic studies of *A1* and *A3* cytotoxicity in MDA-MB-231 cells

Next we conducted mechanistic studies to gain insights into the

cellular targets of the acridinium-based ILs. Previous studies have shown that ILs exert their cytotoxic effects by permeabilising cellular membranes and/or inducing mitochondrial dysfunction [6,10,11,16,18,19,26,27]. Mitochondria mediate important cellular processes including the regulation of reactive oxygen species (ROS) and biosynthesis of adenosine triphosphate (ATP) from fatty acids and other nutrients. ATP synthesis occurs via oxidative phosphorylation (OXPHOS), a process in which the electron transport chain pumps protons across the inner mitochondrial membrane (IMM). The resulting mitochondrial membrane potential ($\Delta\Psi_m$) is used to catalyse ATP production by ATP synthase [28]. We have recently provided evidence that AmILs with aromatic head groups rapidly accumulate in mitochondria and permeabilise the IMM at cytotoxic concentrations, leading to an inhibition of ATP synthesis by OXPHOS, and increased production of cellular ROS [10,16]. Mitochondrial accumulation of aromatic cations in the IMM occurs from the interaction of the cation with $\Delta\Psi_m$, and because delocalisation of the positive charge across the head group renders the cation sufficiently lipophilic to diffuse through cellular membranes to access mitochondria. Mechanistic studies therefore assessed the capacity of acridinium-based AmILs **A1** and **A3** to disrupt lipid bilayers and mitochondrial function, and their effects were compared to [C_{16}Py][I], which we have established to target the IMM [16].

To investigate their effects on membrane integrity, tethered bilayer lipid membranes (tBLMs) – solid-supported membranes anchored between gold electrodes – were treated with **A1**, **A3** and [C_{16}Py][I] and changes in membrane permeability were detected changes in ionic conductance [21]. For these experiments, tBLMs were assembled with DOPC since it is one of the most abundant phospholipids found in the IMMs of mammalian cells [29]. As shown in Fig. 2, **A3** produced a rapid increase in membrane conductance that reached 12000 % of control within 7 min. Under the same conditions, [C_{16}Py][I] increased membrane conductance to ~ 700 % of control, while **A1** produced the smallest effect. The membrane disrupting effects of [C_{16}Py][I], **A1** and **A3** reflect their MTS IC_{50} concentrations, and suggest that these AmILs reduce cell viability by targeting cellular membranes.

Our previous studies have shown that [C_{16}Py][I]-mediated permeabilisation of the IMM inhibits OXPHOS, decreases ATP production, and induces ROS formation [16]. We therefore assessed the capacity of **A1** and **A3** to induce mitochondrial dysfunction in MDA-MB-231 cells. For these assays, cells were treated with AmILs for short time periods to observe early cellular events likely associated with their cytotoxicity.

The effects of the ILs on mitochondrial function in MDA-MB-231 cells was first assessed using the Seahorse Mito Stress test. This assay detects changes in cellular oxygen consumption rate (OCR) and extracellular acidification rate (ECAR), which are proportional to the rates of OXPHOS and glycolysis, respectively. Treatment of MDA-MB-231 cells with [C_{16}Py][I] leads to a rapid decrease in OCR and increase in ECAR, consistent with inhibition of OXPHOS and a shift towards glycolysis to meet cellular ATP demands (see Fig. 3A and **B**). [C_{16}Py][I] also strongly reduces maximal respiration (see Fig. 3C), which reflects the functional status of the electron transport chain embedded in the IMM and is an indicator of mitochondrial dysfunction. In contrast, the acridinium-based AmIL **A1** did not alter OCR and ECAR relative to DMSO-treated control cells (see Fig. 3). The effects of the phenylacridinium-based AmIL **A3** were similar to those of **A1**, although a modest reduction in maximal respiration relative to that produced by [C_{16}Py][I] was observed. These findings suggest that unlike [C_{16}Py][I], AmILs **A1** and **A3** do not affect mitochondrial function in MDA-MB-231 cells at their MTS IC_{50} concentrations.

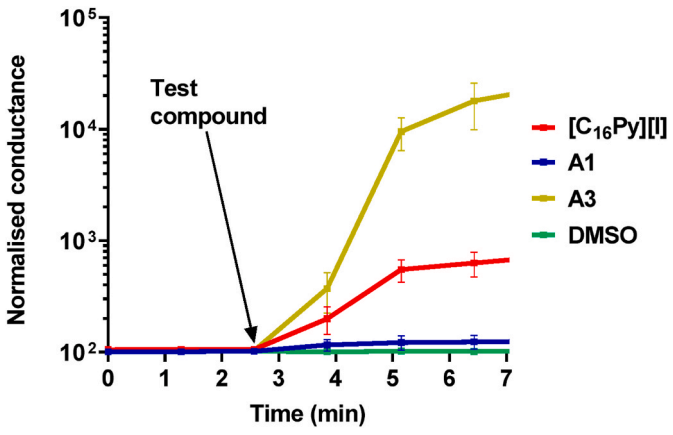

Fig. 2. The effects of [C_{16}Py][I], **A1** and **A3** (10 μM) on the ionic conductance of DOPC lipid bilayers tethered to gold electrodes as measured by electrical impedance spectroscopy. Data were normalised to a baseline control and represent the mean ± SEM from 3 independent experiments. Values for [C_{16}Py][I] taken from previously reported data [16].

In respiring mitochondria, a proton gradient across the IMM generates the mitochondrial membrane potential ($\Delta\Psi_m$), which is harnessed to sustain ATP synthesis via OXPHOS [28]. To assess the effects of **A1** and **A3** on $\Delta\Psi_m$, we performed JC-1 assays with MDA-MB-231 cells. JC-1 is a redox-active dye that aggregates in mitochondria with high $\Delta\Psi_m$ and fluoresces reds. In response to the loss of $\Delta\Psi_m$, JC-1 dissociates to monomers in the cytosol that fluoresce green. The ratio of JC-1 red/green fluorescence can therefore be used to measure $\Delta\Psi_m$, and JC-1 IC_{50} values were determined as concentrations required to shift the red/green fluorescence ratio by 50 % (see Fig. S2 in Supporting Information). Maximum effect (E_{max}) values were used indicate maximum shifts in red/green fluorescence produced by the AmILs. As shown in Table 2 (see Fig. S3 in Supporting Information for dose-response curves), [C_{16}Py][I] produced a JC-1 IC_{50} concentration of 7.9 ± 0.4 μM, which is comparable to its MTS IC_{50} of 7.7 ± 0.3 μM and indicates that collapse of $\Delta\Psi_m$ is associated with AmIL-mediated reductions in cell viability [16]. Both **A1** and **A3** also affected the JC-1 red/green fluorescence ratio, however with IC_{50} concentrations significantly higher than their MTS IC_{50} concentrations (see Table 2). **A1** also had a high E_{max} value, suggesting that **A1** has a limited effect on $\Delta\Psi_m$ even at very high concentrations.

Inhibition of OXPHOS and collapse of $\Delta\Psi_m$ can lead to a reduction in ATP synthesis. Therefore intracellular ATP levels in MDA-MB-231 cells treated with **A1** and **A3** were monitored over 6 h and compared to [C_{16}Py][I] (see Fig. 4A), which we have shown reduces ATP production in MDA-MB-231 cells [16]. Prior to undertaking these studies, lactate dehydrogenase (LDH) release assays were performed under the same conditions (6 h treatment) to establish if the ILs induced cell death at these time points. This was done so that decreases in ATP could be attributed to the inhibition of OXPHOS rather than loss of cell viability. As shown in Table S1 in the Supporting Information, **A1** did not induce LDH release over 6 h while **A3** did. Thus, the effects of **A1** on ATP levels were monitored over 6 h, and only for 4 h with **A3**. Under these conditions it was found that both **A1** and **A3** did not produce statistically significant reductions in intracellular ATP levels relative to DMSO-treated control cells, in contrast to [C_{16}Py][I].

We next assessed the capacity of **A1** and **A3** to initiate cellular ROS generation in MDA-MB-231 cells using the DCFDA assay. Mitochondria are sites of cellular ROS production [28], and previous studies suggest that ILs may kill cells by promoting excess ROS production [10,11,16,18,19]. Possible mechanisms for IL-mediated ROS production include permeabilisation of the IMM and/or interaction of the IL cation with the electron transport chain [6,10]. As shown in Fig. 4B, acridinium AmILs **A1** and **A3** do not significantly increase cellular ROS production relative to DMSO-treated control cells over 6 h. In contrast, [C_{16}Py][I] produced significant increases in ROS after 4 h that reached ~ 1.6-fold of control after 6 h.

Together the mitochondrial assays suggest that, unlike other aromatic AmILs such as [C_{16}Py][I] [6,10], **A1** and **A3** do not target the IMM to induce mitochondrial dysfunction. Thus, **A1** and **A3** failed to inhibit OXPHOS and promote glycolysis in seahorse assays and did not produce

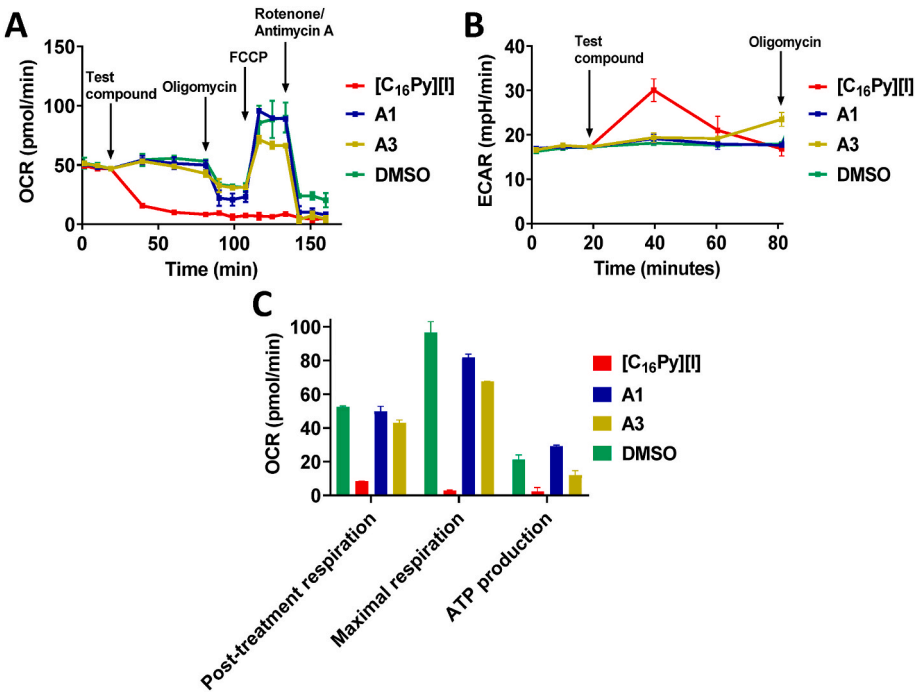

Fig. 3. The effects of [C_{16}Py][I] (7.7 μM), **A1** (57 μM) and **A3** (0.76 μM) mitochondrial function in MDA-MB-231 cells measured using a Seahorse XFe24 Analyser. **A** Oxygen consumption rates of cells treated with sequential additions of the AmILs at their MTS IC_{50} concentrations, followed by oligomycin (1 μM), FCCP (2 μM), and rotenone/Antimycin A (1 μM).[a] **B** ECAR of MDA-MB-231 cells following treatment with [C_{16}Py][I], **A1** and **A3** at their MTS IC_{50} concentrations.[a] **C** OCR parameters associated with post-treatment respiration, maximal respiration, and ATP production in MDA-MB-231 cells following treatment of [C_{16}Py][I], **A1** and **A3**.[a] Data were normalised to a baseline control and represent the mean of 2 separate wells from the same experiment. [a] Values for [C_{16}Py][I] taken from previously reported data [16].

Table 2
Relative IC_{50} concentrations and maximum effect (E_{max}) values of [C_{16}Py][I], **A1** and **A3** (1 h treatment) measured in JC-1 assays.

Cmpd	JC-1 IC_{50} [μM]	E_{max}
[C_{16}Py] [I]	7.9 ± 0.4[a]	24.9 ± 2.5 %[a]
A1	75.8 ± 4.3	66.0 ± 3.3 %
A3	3.5 ± 0.46	34.2 ± 3.3 %

[a] Values taken from previously reported data [16].

significant changes in intracellular ATP or ROS levels. To further interrogate the role of OXPHOS in the cytotoxic effects of [C_{16}Py][I], **A1**, and **A3**, MTS assays were repeated in media supplemented with additional glucose (4.5 g/L, increased from 1 g/L). As shown in Fig. S3 (see Supporting Information), additional glucose in the assay media failed to protect MDA-MB-231 cells from [C_{16}Py][I], **A1**, and **A3**-mediated cytotoxicity, suggesting that inhibition of OXPHOS may not play a central role in the cytotoxic effects of [C_{16}Py][I], **A1** and **A3**. In the case of [C_{16}Py][I], increased ROS production may mediate loss of cell viability.

That **A1** and **A3** do not induce mitochondrial dysfunction is surprising as they carry a delocalised positive charge and are expected to accumulate in the IMM similarly to other delocalised lipophilic cations [10,16,30–33], and because the moderate activity of **A1** and **A3** in JC-1 assays indicates that these AmILs can reduce $\Delta\Psi_m$. Shifts in $\Delta\Psi_m$ can however occur as lipophilic cations accumulate in the mitochondrial matrix rather than the IMM [33]. The mitochondrial matrix is also the site of mitochondrial DNA (mtDNA), and it is possible that **A1** and **A3** reduce cell viability by intercalating to mtDNA. Indeed, structurally related cytotoxic molecules such as ethidium bromide operate by this mechanism [34]. Targeting of mtDNA by the acridinium-based ILs could

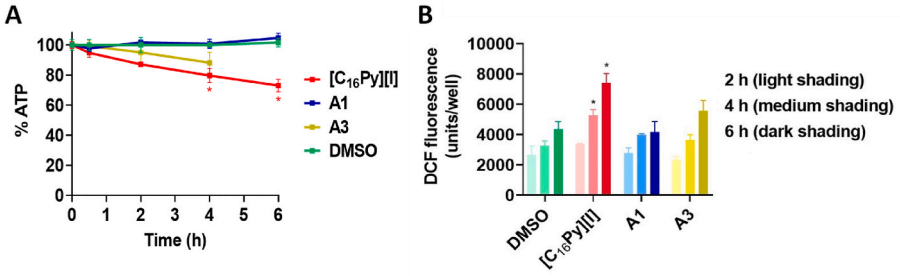

Fig. 4. The effects of [C_{16}Py][I] (7.9 μM), **A1** (75 μM) and **A3** (3.5 μM) on intracellular ATP and cellular ROS levels in MDA-MB-231 cells. **A** Quantification of total intracellular ATP content in MDA-MB-231 cells following treatment with [C_{16}Py][I], **A1** and **A3** at their JC-1 IC_{50} concentrations.[a] Data represent the mean ± SEM of time-matched DMSO controls from 3 independent experiments performed in triplicate. Significantly different from DMSO control: (*) $p < 0.05$. 6 h data point for **A3** not shown due to observed reductions in cell viability. **B** ROS production in MDA-MB-231 cells following treatment with [C_{16}Py][I], **A1** and **A3** at their JC-1 IC_{50} concentrations.[a] Data represent the mean ± SEM from 3 independent experiments performed in triplicate. Significantly different from DMSO control: (*) $p < 0.05$. [a] Values for [C_{16}Py][I] taken from previously reported data [16].

also explain some of the SAR findings from the MTS assays. Firstly, the MTS data showed that the length of the *N*-alkyl side chain had minimal impact on the cytotoxicity of the acridinium-based ILs (see **A19**–**23**), which is unusual as all previous studies have consistently shown that lengthening the *N*-alkyl chain produces dramatic increases in IL cytotoxicity [5–12]. For example, increasing the decyl chain length of the methylimidazolium IL [C_{10}MIM][Cl] by 6 carbons to [C_{16}MIM][Cl] resulted in a 3-fold increase in cytotoxicity. The correlation between IL cytotoxicity and *N*-alkyl chain length is thought to occur because ILs target cellular membranes [15,26,27]. Thus the SAR suggests that acridinium-based ILs produce cytotoxicity by a different mechanism. Secondly, substitution of the phenyl-acridinium head group with methyl groups had negligible effects on cytotoxicity, except when a methyl group was placed in the *ortho*-position (see **A14**). This is consistent with DNA targeting as the *ortho*-methyl group in **A14** can act as a conformation blocker that locks the phenyl and acridinium rings out-of-plane with each other, forcing **A14** into a configuration that is less able to intercalate between base-pairs in DNA.

To provide some experimental evidence to support this we studied the interaction of [C_{16}Py][I], **A1**, and **A3** with calf thymus DNA (CT-DNA) by UV–Visible absorption spectroscopy [35,36]. **A1** and **A3** bound to CT-DNA with association constants (K_a) of 9.3×10^4 M^{-1} and 2.8×10^3 M^{-1}, respectively, and are comparable to that of ethidium bromide ($K_a = 130 \times 10^4$ M^{-1} with double-stranded DNA) [34]. Hyperchromic shifts in the CT-DNA absorption band at 260 nm produced by **A1** and **A3** are consistent with DNA intercalation (see Figs. S4–6 in Supporting Information). [C_{16}Py][I] also produced similar effects but with an association constant 1-2 orders of magnitude lower than those of **A1** and **A3.**

4. Conclusions

In summary, the data presented here shows 9-phenylacridinium-based ILs are cytotoxic agents that are approximately 10-fold more potent that the corresponding pyridinium-based IL. Cytotoxicity was only moderately affected by substitution of the head group, and decreased as the *N*-alkyl side chain was lengthened. Mechanistic studies showed that 9-phenylacridinium-based ILs do not produce the same mitochondrial effects as [C_{16}Py][I], and it is possible that these ILs may interact with mtDNA to reduce the viability of MDA-MB-231 cells.

CRediT authorship contribution statement

Ritik Roy: Writing – review & editing, Writing – original draft, Methodology, Investigation, Formal analysis, Data curation. **Phoenix Chick:** Formal analysis, Investigation, Methodology, Visualization. **Edward York:** Formal analysis, Investigation, Methodology, Visualization. **Tristan Rawling:** Writing – review & editing, Writing – original draft, Supervision, Project administration, Methodology, Formal analysis, Conceptualization.

Declaration of competing interest

The authors declare that they have no known competing financial interests or personal relationships that could have appeared to influence the work reported in this paper.

Data availability

Data will be made available on request.

Acknowledgments

This research was supported by an Australian Government Research Training Program Scholarship.

Appendix A. Supplementary data

Supplementary data to this article can be found online at https://doi.org/10.1016/j.cbi.2024.111042.

References

[1] K. Goossens, K. Lava, C. Bielawski, K. Binnemans, Ionic liquid crystals: versatile materials, Chem. Rev. 116 (8) (2016) 4643–4807.
[2] J. Song, Research progress of ionic liquids as lubricants, ACS Omega 6 (44) (2021) 29345–29349.
[3] Z. Fang, X. Zheng, L. Li, J. Qi, W. Wu, Y. Lu, Ionic liquids: emerging antimicrobial agents, Pharmaceut. Res. 39 (10) (2022) 2391–2404.
[4] C. Pretti, C. Chiappe, D. Pieraccini, M. Gregori, F. Abramo, G. Monni, L. Intorre, Acute toxicity of ionic liquids to the zebrafish (*Danio rerio*), Green Chem. 8 (2005) 238–240.
[5] R. Bernot, E. Kennedy, G. Lamberti, Effects of ionic liquids on the survival, movement, and feeding behaviour of the freshwater snail, *Physa acuta*, Environ. Toxicol. Chem. 24 (7) (2005) 1759–1765.
[6] T. Abdelghany, A. Lietch, A. Nevjestic, I. Ibrahim, S. Miwa, C. Wilson, S. Heutz, M. Wright, Emerging risk from "environmentally friendly" solvents: interaction of methylimidazolium ionic liquids with the mitochondrial electron transport chain is a key initiation event in their mammalian toxicity, Food Chem. Toxicol. 145 (2020) 1–14.
[7] S. Pérez, M. Montalbán, G. Carissimi, P. Licence, G. Víllora, *In vitro* cytotoxicity assessment of monocationic and dicationic pyridinium-based ionic liquids on HeLa, MCF-7, BGM and EA.hy926 cell lines, J. Hazard Mater. 385 (2020) 1–9.
[8] M. McLaughlin, M. Earle, M. Gîlea, B. Gilmore, S. Gorman, K. Seddon, Cytotoxicity of 1-alkylquinolinium bromide ionic liquids in murine NIH 3T3 cells, Green Chem. 13 (10) (2011) 2794–2800.
[9] U. Dzhemileva, V. D'yakonov, M. Seitkalieva, N. Kulikovskaya, K. Egorova, V. Ananikov, A large-scale study of ionic liquids employed in chemistry and energy research to reveal cytotoxicity mechanisms and to develop a safe design guide, Green Chem. 23 (17) (2021) 6414–6643.
[10] M.N. Duman, A. Angeloski, M. Johnson, T. Rawling, Aromatic long chain cations of amphiphilic ionic liquids permeabilise the mitochondrial inner membrane and induce mitochondrial dysfunction at cytotoxic concentrations, Green Chem. 25 (2023) 6067–6076.
[11] X. Li, J. Ma, J. Wang, Cytotoxicity, oxidative stress, and apoptosis in HepG2 cells induced by ionic liquid 1-methyl-3-octylimidazolium bromide, Ecotoxicol. Environ. Saf. 120 (2015) 342–348.
[12] R. Frade, A. Matias, L. Branco, C. Alfonso, C. Duarte, Effect of ionic liquids on human colon cancer carcinoma HT-29 and CaCo-2 cell lines, Green Chem. 9 (2007) 873–877.
[13] S. Farahani, M. Sohrabi, J. Ghasemi, A detailed structural study of cytotoxicity effect of ionic liquids on the leukemia rat cell line IPC-81 by three dimensional quantitative structure toxicity relationship, Ecotoxicol. Environ. Saf. 158 (2018) 256–265.
[14] S. Stolte, J. Arning, U. Bottin-Webber, M. Matzke, F. Stock, K. Thiele, M. Uerdingen, Jastorff B. Welz-Biermann, J. Ranke, Anion effects on the cytotoxicity of ionic liquids, Green Chem. 8 (2006) 621–629.
[15] N. Kaur, M. Fischer, S. Kumar, G.K. Gahlay, H. Scheidt, V.S. Mithu, Role of cationic head-group in cytotoxicity of ionic liquids: probing changes in bilayer architecture using solid-state NMR spectroscopy, J. Colloid Interface Sci. 581 (2021) 954–963.
[16] R. Roy, E. York, E. Pacchini, T. Rawling, Effects of cationic head group structure on cytotoxicity and mitochondrial actions of amphiphilic ionic liquids, Food Chem. Toxicol. 183 (2024) 1–8.
[17] Y. Zhou, J. Qu, Ionic liquids as lubricant additives: a review, ACS Appl. Mater. Interfaces 9 (4) (2017) 3209–3222.
[18] L. Hu, Q. Xiong, W. Shi, G. Huang, Y. Liu, G. Ying, New insight into the negative impact of imidazolium-based ionic liquid [C10mim]Cl on HeLa cells: from membrane damage to biochemical alterations, Ecotoxicol. Environ. Saf. 208 (2021) 1–12.
[19] J. Ma, X. Li, Insight into the negative impact of ionic liquid: a cytotoxicity mechanism of 1-methyl-3-octylimidazolium bromide, Environ. Pollut. 285 (2018) 1337–1345.
[20] G. Pauli, S.N. Chen, C. Simmler, D. Lankin, T. Gödecke, B. Jaki, B.F. Friesen, J. McAlpine, J. Napolitano, Importance of purity evaluation and the potential of quantitative ^{1}H NMR as a purity assay, J. Med. Chem. 58 (22) (2014) 9220–9231.
[21] C. Cranfield, S. Carne, B. Martinac, B. Cornell, The assembly and use of tethered bilayer lipid membranes (tBLMs), Methods Mol. Biol. 1232 (2015) 45–53.
[22] C. Cranfield, S. Henriques, B. Martinac, P. Duckworth, D. Craik, B. Cornell, Kalata B1 and kalata B2 have a surfactant-like activity in phosphatidylethanolamine-containing lipid membranes, Langmuir 33 (26) (2017) 6630–6637.
[23] R. Martin, S. Buchwald, Palladium-catalyzed suzuki–miyaura cross-coupling reactions employing dialkylbiaryl phosphine ligands, Accounts Chem. Res. 41 (11) (2008) 1461–1473.
[24] D. Mital, P. Nancarrow, T. Ibrahim, N. Jabbar, M. Khamis, Ionic liquid melting points: structure–property analysis and new hybrid group contribution model, Ind. Eng. Chem. Res. 61 (13) (2022) 4683–4706.
[25] Y. Zhang, E. Maginn, Molecular dynamics study of the effect of alkyl chain length on melting points of [C_nMIM][PF_6] ionic liquids, Phys. Chem. Chem. Phys. 16 (26) (2014) 13489–13499.

[26] K. Bakshi, S. Mitra, V. Sharma, M. Jayadev, V. Sakai, R. Mukhopadhyay, A. Gupta, S. Ghosh, Imidazolium-based ionic liquids cause mammalian cell death due to modulated structures and dynamics of cellular membranes, Biochim. Biophys. Acta Biomembr. 1862 (2) (2020) 1–11.
[27] S. Kumar, H. Scheidt, N. Kaur, T. Kang, G. Gahlay, D. Huster, V. Mithu, Effect of the alkyl chain length of amphiphilic ionic liquids on the structure and dynamics of model lipid membranes, Langmuir 35 (37) (2019) 12215–12223.
[28] M. Giacomello, A. Pyakurel, C. Glytsou, L. Scorrano, The cell biology of mitochondrial membrane dynamics, Nat. Rev. Mol. Cell Biol. 21 (4) (2020) 204–224.
[29] S.E. Horvath, G. Daum, Lipids of mitochondria, Prog. Lipid Res. 52 (4) (2013) 590–614.
[30] J. Zielonka, J. Jospeh, A. Sikora, M. Hardy, O. Ouari, J. Vasquez-Vivar, G. Cheng, M. Lopez, B. Kalyanaraman, Mitochondria-targeted triphenylphosphonium-based compounds: syntheses, mechanisms of action, and therapeutic and diagnostic applications, Chem. Rev. 117 (15) (2017) 10043–10120.
[31] P. Lu, B. Bruno, M. Rabenau, C. Lim, Delivery of drugs and macromolecules to the mitochondria for cancer therapy, J. Contr. Release 240 (2016) 38–51.
[32] M. Murphy, R. Smith, Targeting antioxidants to mitochondria by conjugation to lipophilic cations, Annu. Rev. Pharmacol. Toxicol. 47 (1) (2007) 629–656.
[33] H. Rottenberg, Membrane potential and surface potential in mitochondria: uptake and binding of lipophilic cations, J. Membr. Biol. 81 (2) (1984) 127–138.
[34] P. Vardevanyan, A. Antonyan, M. Parsadanyan, H. Davtyan, A. Karapetyan, The binding of ethidium bromide with DNA: interaction with single- and double-stranded structures, Exp. Mol. Med. 35 (6) (2003) 527–533.
[35] M. Sirajuddin, S. Ali, A. Badshah, Drug-DNA interactions and their study by UV-Visible, fluorescence spectroscopies and cyclic voltammetry, J. Photochem. Photobiol. B Biol. 124 (2013) 1–19.
[36] S. Yasmeen, F. Qais, M. Rana, A. Islam, Rahisuddin, Binding and thermodynamic study of thalidomide with calf thymus DNA: spectroscopic and computational approaches, Int. J. Biol. Macromol. 207 (2022) 644–655.